



Open Archive TOULOUSE Archive Ouverte (OATAO)

OATAO is an open access repository that collects the work of Toulouse researchers and makes it freely available over the web where possible.

This is an author-deposited version published in : <http://oatao.univ-toulouse.fr/>
Eprints ID : 18368

To link to this article : DOI: 10.1051/kmae/2016032
URL : <http://dx.doi.org/10.1051/kmae/2016032>

<p>To cite this version : Cassan, Ludovic and Laurens, Pascale <i>Design of emergent and submerged rock-ramp fish passes</i>. (2016) Knowledge and Management of Aquatic Ecosystems, vol. 417 (n° 45). pp. 1-10. ISSN 1961-9502</p>
--

Any correspondence concerning this service should be sent to the repository administrator: staff-oatao@listes-diff.inp-toulouse.fr

RESEARCH PAPER

OPEN ACCESS

Design of emergent and submerged rock-ramp fish passes

Ludovic Cassan* and Pascale Laurens

Institut de Mécanique des Fluides, allée du Prof. Camille Soula, 31400 Toulouse, France

Abstract – An analytical model is developed to calculate the stage-discharge relationship for emergent and submerged rock-ramp fish passes. A previous model has been modified and simplified to be adapted to a larger range of block arrangement. For submerged flows, a two-layer model developed for aquatic canopies is used. A turbulent length scale is proposed to close the turbulence model thanks to a large quantity of data for fully rough flows from the literature and experiments. This length scale depends only on the characteristic lengths of arrangements of obstacles. Then the coefficients of the logarithmic law above the canopy can also be deduced from the model. As a consequence, the total discharge through the fish pass is computed by integrating the vertical velocity profiles. A good fit is found between the model and commonly observed values for fish pass or a vegetated canopy. The discharge of the fish pass is then accurately estimated for a large range of hydraulic conditions, which could be useful for estimating fish passability through the structure.

Keywords: rock-ramp / fishpass / design / hydraulic resistance / turbulence

Résumé – Dimensionnement de passes à poissons constituées de rampes à macrorugosités émergées et immergées. Un modèle analytique a été développé pour déterminer la relation de dimensionnement de passes à poissons constituées de rampes à macrorugosités émergées et immergées. Un modèle proposé précédemment a été modifié et simplifié afin de couvrir un éventail plus large de configurations géométriques. Pour des macrorugosités immergées, un modèle à deux couches pour des écoulements au-dessus de végétation, a été utilisé. Grâce à l'analyse de nos données et à celles de la littérature, une expression de la longueur de mélange est obtenue afin de fermer le modèle de turbulence. Cette longueur de mélange est basée uniquement sur les longueurs caractéristiques de l'arrangement des macrorugosités. Les coefficients de la loi logarithmique des vitesses au-dessus des obstacles sont alors déduits ce qui fournit le débit total par intégration du profil vertical de vitesse. Le modèle fournit une bonne estimation des vitesses et des débits par rapports aux données expérimentales. Ainsi une relation hauteur-débit est calculable pour des conditions géométriques et hydrologiques très variées ce qui est primordial pour estimer la franchissabilité de ces ouvrages.

Mots clés : macrorugosités / fortes pentes / passes à poissons / modèle analytique

1 Introduction

Over the last twenty years, there have been many plans to restore the populations of migratory fish species (*e.g.* salmon, sea-trout, shad, lamprey) in France's waterways. More recently, holobiotic species (*e.g.* barbel, riverine trout, nase) are also more and more taken into account. One of the necessary measures involves re-establishing the connectivity along these waterways and in particular the passage of fish at obstacles (weirs and dams). In general, according to all the fishway design guidelines and taking into account the specific biological constraints, it is possible to design any type of fishway for most species and life stages presented in a

river reach (FAO, 2002; Larinier *et al.*, 2006a). However, engineering and economic constraints make only possible to design some types, such as technical fishways, for species with good swimming abilities. In addition, technical fishways (*e.g.* pool and weir or vertical slot fishways) are usually built with more frequency than nature-like fishways (bypass channels or rock-ramps) due to its shorter topographic development. Nevertheless, for small weirs (height mostly lower than 2–3 m), rock-ramp passes are being developed (Baki *et al.*, 2014) and can have some advantages: possibility of high discharges interesting for the attractiveness of the facility and a lower sensitivity than technical fishways to clogging by floating debris and sediments. Three types of rock ramps can be encountered: (i) rough rock-ramp, (ii) rock-ramp with perturbation boulders and (iii) step-pool rock-ramp. In this paper the second type is studied for both emergent and

*Corresponding author: lcassan@imft.fr

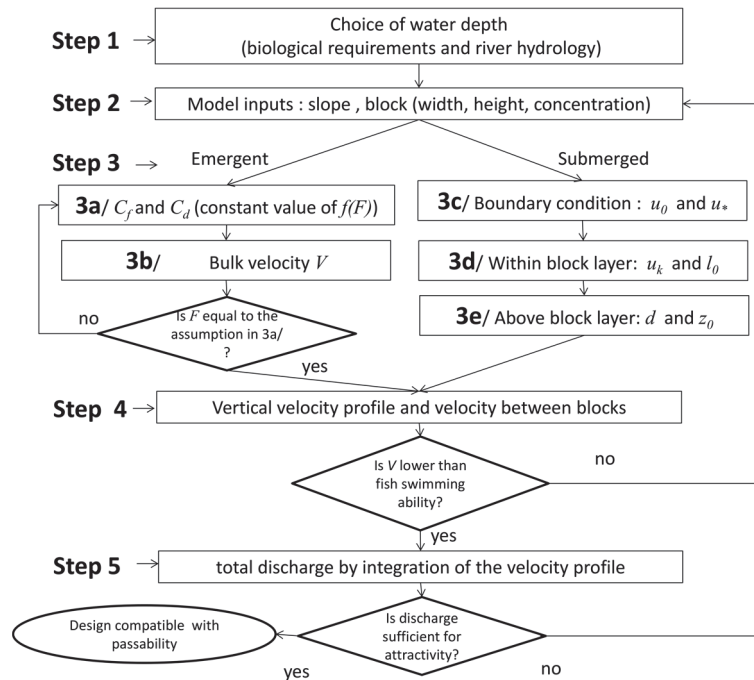


Fig. 1. Flow chart of the design method.

submerged condition of perturbation boulders. Indeed, fishways have to be functional over a wide range of river flow and thus have to be adapted to the variations of upstream and downstream water levels. This is the reason why rock ramps usually have a half V-profile section. Within a ramp, there may be sub-sections where the blocks are submerged and others sub-sections where the blocks are emergent, depending on the upstream water level. In practice, blocks can be submerged with heights of water up to twice their height at the higher river flow of the functionality range (Larinier *et al.*, 2006b). The submergence of some sub-sections of a ramp results in a rapid increase in their discharge and is interesting for the attractiveness of the facility, while more gentle hydraulic conditions are maintained in emergent sub-sections. The submerged sub-sections may also remain passable at least at low submergence and for species with high swimming capacities, but up to now, there was no model to compute the flow velocities in each flow layer (between blocks and above blocks). In Cassan *et al.* (2014), an analytical model was firstly developed for emergent rock-ramp fish pass, where the contribution of drag and bed on energy dissipation was quantified. Compared to previous methods (FAO, 2002; Heimerl *et al.*, 2008), the evolution of the boulder drag coefficient can be estimated as a function of hydraulic parameters (Froude number, block shape and slope).

The first objective of this study is to propose a simpler version of the model proposed by Cassan *et al.* (2014) for emergent ramps, and to extend its relevance to blocks' arrangements with transverse and longitudinal spaces between blocks that are uneven. This is based on new experiments results obtained on a down-scale physical model and on the comparison with other models from bibliography.

The second and main objective is to develop an analytical model for submerged ramps to estimate the stage-discharge relationship and the velocities in the different flow layers. This

model is adapted from one-dimensional vertical models developed for vegetation (Klopstra *et al.*, 1997; Huthoff *et al.*, 2007; Murphy and Nepf, 2007; King *et al.*, 2012), and by analyzing experiments results obtained on a down-scale physical model. Vegetation models usually study the turbulent flow as a function of the geometry, being comparable with submerged rock-ramps. The difficulty in these models arises in simulating the total turbulence intensity based on the configuration of the flow (arrangement of obstacles, slope and flow rate). Here, a turbulence closure model is proposed to estimate vertical velocity profiles and the turbulent viscosity for a large range of blocks arrangements. The proposed model is also compared to existing experimental stage-discharge correlations (Larinier *et al.*, 2006b; Heimerl *et al.*, 2008; Pagliara *et al.*, 2008).

2 Method

In this part, the experimental device is firstly presented. Secondly, the method described in Figure 1 to design a rock-ramp fish pass, is proposed and each step is detailed in the following paragraphs. After the choice of water depth, slope and block (steps 1 and 2), experiments were performed to establish relationships for the velocity computation (step 3). The last steps consist in checking the passability and adjusting the design if necessary (steps 4 and 5). Some theoretical aspects are included in the corresponding step whereas the experiments analysis leading to the design formula is presented in the results part.

2.1 Experimental device

The fish pass is modeled as an arrangement of blocks (or macro-roughness) spaced regularly in the transverse (a_x) and longitudinal (a_z) directions (Cassan *et al.*, 2014). The

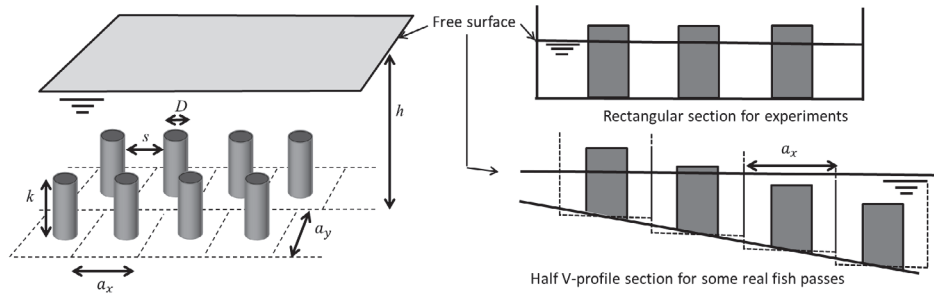


Fig. 2. Definition of geometric variables for experiments (left) and view of the transverse section for real scale fishway (right). The water flows in the y -direction.

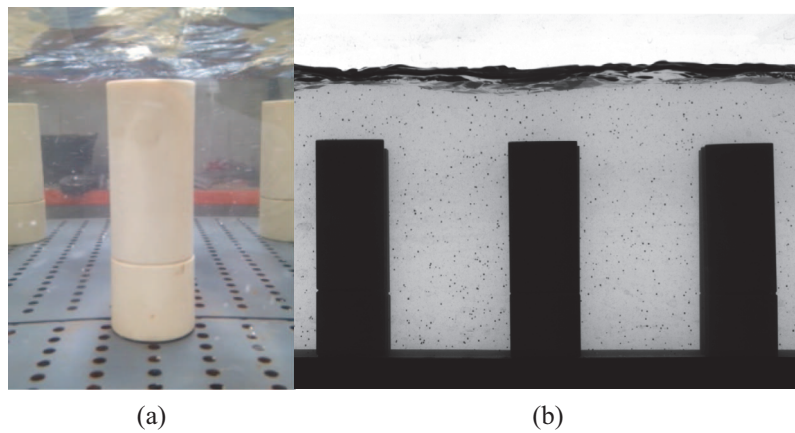


Fig. 3. Photography of one block (a) and instantaneous picture of the flow for $k=0.1$ m, $S=0.01$ and $C=0.1$ (b).

arrangement is expressed with the concentration $C = D^2/a_x a_y$, where D is the characteristic width facing the flow. The blocks are defined by D , by their height k , and by the minimum distance between them, $s = D(1/C^{1/2} - 1)$ (Fig. 2). The averaged water depth is denoted h .

The experiments were carried out on a rectangular channel (0.4 m wide and 4.0 m long) with a variable slope. The macro-roughness consisted of plastic cylinders 0.035 m in diameter with a height (k) of either 0.03 m, 0.07 m or 0.1 m. The blocks were arranged in a staggered pattern with several densities (see Tab. 1 and Fig. 2). For experiments, the bed is horizontal in the transverse direction even if it can be sloped for some real scale fishways. The bed was covered by Polyvinyl chloride plate. A camera (1024×1280 pixels) was used to view the free surface of a pattern, using shadowscopy and a LED lighting system to differentiate the air from the water (Fig. 3). The image-acquisition frequency was 3 Hz and a series of 50 images were taken for each flow rate. The time-averaged water depth in the transverse direction (compared to the water's direction) was provided by the position of the minimum signal. The mean water depth (h) on the pattern was then deduced by integrating the free surface in the longitudinal direction. Flow rates were measured using KROHNE electromagnetic flow meters, accurate to 0.5%. Tests were carried out with slopes (S) of 1, 2, 3, 4 and 5% for all arrangements (Tab. 1). The flow rates for each slope were between $0.001 \text{ m}^3 \text{ s}^{-1}$ and $0.018 \text{ m}^3 \text{ s}^{-1}$ with a $0.002 \text{ m}^3 \text{ s}^{-1}$ step. The performance of flow (emergent or submerged) depends on the discharge and the slope (see Supplementary data).

2.2 Step 1 and 2: Geometrical characteristics

The block arrangements are depicted in Figure 2. They are characterized by D , k and C . The ratio between water depth and the characteristic width is denoted by $h_* = h/D$. Cassan *et al.* (2014) emphasized that the flow pattern depends on the Froude number $F = V_g/\sqrt{gh}$ (g is the gravitational acceleration) based on the averaged velocity between blocks V_g (Eq. (1)).

$$\frac{V_g}{V} = \frac{1}{1 - \sqrt{(a_x/a_y)C}}, \quad (1)$$

where V is the bulk velocity, *i.e.* the total discharge divided by the ramp width and by h . The cross section is rectangular for experiments and for this theoretical approach. However some fish passes have a half V-profile section. They can be approximated as several rectangular sub-sections juxtaposed in the transverse direction. The method is applied for each sub-section and the water depth is modified as a function of the bed level. The design relationships remain relevant if the influence of the lateral slope on the transverse transfers is neglected (Fig. 2). The validation of this assumption is given by *in situ* measurement available in Tran (2015) for emergent condition.

2.3 Step 3: Computation of velocity

2.3.1 Step 3a and 3b

To compute the stage-discharge relationship for emergent performance, the flow analysis is based on the momentum

Table 1. Geometrical description of experiments. Slopes of 1, 2, 3, 4 and 5% for all arrangements.

Exp	$D(m)$	C	$a_x(m)$	$a_y(m)$	a_y/a_x
E1	0.035	0.080	0.110	0.140	1.27
E2	0.035	0.130	0.090	0.120	1.33
E3	0.035	0.190	0.110	0.060	0.54
E4	0.035	0.190	0.080	0.080	1
E5	0.035	0.095	0.080	0.160	2
E6	0.035	0.100	0.110	0.110	1
E7	0.035	0.050	0.110	0.220	2

balance applied on a cell ($a_x \times a_y$) around one block where resistance forces are equal to the gravity force. In [Cassan et al. \(2014\)](#), as the flow around a block is influenced by other blocks and the bed, the drag coefficient was decomposed by three functions $f_C(C)$, $f_F(F)$ and $f_{h_*}(h_*)$ ($C_d = C_{d0}f_C(C)f_F(F)f_{h_*}(h_*)$) where C_{d0} is the drag coefficient of a single, infinitely long block with $F \ll 1$, S is the bed slope) which allow taking into account the concentration, Froude number and aspect ratio influences. As a consequence the momentum balance can be written in a dimensionless form as follows:

$$C_{d0}f_C(C)f_F(F)f_{h_*}(h_*)\frac{Ch}{D}\left(\frac{1+N}{1-\sigma C}\right)F^2 = 2S, \quad (2)$$

with $N = (\alpha C_f)/(C_d Ch_*)$ and $\alpha = [(1 - \sqrt{C(a_y/a_x)}) - (1/2)\sigma C]$. N is the ratio between bed friction force and drag force, α is the ratio of the area where the bed friction occurs on $a_x \times a_y$ and σ is the ratio between the block area in the x, y plane and D^2 (for a cylinder $\sigma = \pi/4$), C_f is the bed friction coefficient from [Rice et al. \(1998\)](#) ([Cassan et al., 2014](#)). C_f is calculated by:

$$C_f = \frac{2}{(5.1 \log(h/k_s) + 6)^2}. \quad (3)$$

The roughness parameter (k_s) is assumed to be equal to the mean diameter of pebbles on the bed. A common value for real scale fish pass is $k_s = 0.1$ m ([Tran, 2015](#)).

The influence of concentration on drag coefficient is estimated with a model based on the interaction between two cylinders ([Nepf, 1999](#)). The correction function $f_C(C)$ proposed in [Cassan et al. \(2014\)](#) is only valid for $a_x/a_y \approx 1$ which does not correspond to all the present arrangements. A solution is to assume that $f_C = (V/V_g)^2$, the validity of this hypothesis is discussed in the results part. Then the momentum can be expressed as follows:

$$C_{d0}f_F(F)f_{h_*}(h_*)\frac{Ch}{D}\left(\frac{1+N}{1-\sigma C}\right)F_0^2 = 2S, \quad (4)$$

where F_0 is the Froude number based on h and V .

The function $f_F(F)$ is based on the fact that velocity increases because of the vertical contraction and that it is fixed to the critical velocity when a transition occurs. The analytical expression selected to reproduce these phenomena are the following ([Cassan et al., 2014](#)):

$$f_F(F) = \min\left(\frac{1}{1 - (F^2/4)}, \frac{1}{F^3}\right), \quad (5)$$

$$f_{h_*}(h_*) = 1 + \frac{0.4}{h_*^2}. \quad (6)$$

The bulk velocity of rock-ramp fish pass is done by applying equation (4) with the correction function $f_{h_*}(h_*)$ and $f_F(F)$. The relationship between F and F_0 is deduced from equation (1) and the friction coefficient (C_f) from Rice formula (Eq. (3)).

2.3.2 Step 3c

The model is based on the spatially double-average method developed for atmospheric or aquatic boundary layers ([Klopstra et al., 1997](#); [Lopez and Garcia, 2001](#); [Nikora et al., 2001](#); [Katul et al., 2011](#)) for which the submergence ratio are similar ($h/k \in [1, 3]$). First, the velocity at the bed $u_0 = \sqrt{2gSD(1 - \sigma C)/(C_d C)}$ is computed. As the discharge continuity between emergent and submerged rock-ramp is assumed, the correction f_{h_*} is also applied in the C_d calculation whereas f_F could be neglected. Indeed, when the blocks are submerged the correction function due to the vertical contraction of the flow becomes non significant. Like for emergent conditions, the drag force within the block layer is expressed as a function of the spatially averaged velocity, then the function f_C is also neglected. At the top of the canopy, the total stress τ is computed with the shear velocity $u_* = \sqrt{gS(h - k)}$ ($\tau = \rho u_*^2$ where ρ is the water density).

2.3.3 Step 3d

Within the canopy, an analytical formulation for the velocity u is obtained by modeling τ with the following equation:

$$\tau = \rho \nu_t \frac{du}{dz} = \rho \alpha_t u \frac{du}{dz}, \quad (7)$$

where z is the vertical coordinate, ν_t is the turbulent viscosity, and α_t is a turbulent length scale ([Meijer and Velzen, 1999](#); [Poggi et al., 2009](#)).

The momentum balance in dimensionless form can be written as ([Defina and Bixio, 2005](#)):

$$\frac{1}{\beta^2} \frac{\partial^2 \xi}{\partial \tilde{z}^2} + 1 - \xi = 0, \quad (8)$$

with $\beta^2 = (k/\alpha_t)(C_d C k/D)/(1 - \sigma C)$ is the force ratio between drag and turbulent stress, $\xi = (u/u_0)^2$ is the dimensionless square of the velocity, and $\tilde{z} = z/k$ is the dimensionless

vertical position. Viscous terms are neglected because the Reynolds number $Re = u_0 k / \nu$ (ν is the water kinematic viscosity) is considerably larger than the values used for studies with vegetation (Meijer and Velzen, 1999; Defina and Bixio, 2005). The drag coefficient and diameter are assumed to be constant vertically. Finally, the velocity profile between the blocks can then be expressed by solving equation (8) with the boundary condition $\xi(0) = 1$:

$$u(\tilde{z}) = u_0 \sqrt{\beta \left(\frac{h}{k} - 1 \right) \frac{\sinh(\beta \tilde{z})}{\cosh(\beta)} + 1}. \quad (9)$$

The continuity of the eddy viscosity at the canopy provides the relationship between the turbulent length scale at the top of blocks (l_0) and α_t :

$$l_0 u_* = \alpha_t u_k. \quad (10)$$

In this step, equations (9) and (10) have to be solved simultaneously since u_k (velocity at the top of the canopy) depends on α_t . Using the experimental results (see further), the value of l_0 is given by the following equation:

$$l_0 = \min(s, 0.15 k). \quad (11)$$

2.3.4 Step 3e

The velocity above the canopy is assumed to be logarithmic (Eq. (12)).

$$\frac{u}{u_*} = \frac{1}{\kappa} \ln \left(\frac{z-d}{z_0} \right), \quad (12)$$

where u is the velocity above the canopy, κ the von Karman constant ($\kappa = 0.41$), d the displacement height of the logarithmic velocity profile, and z_0 the hydraulic roughness. A velocity defect law is not used because of low confinements ($h/k < 3$). The continuity of the velocity and the derivative at the top of the canopy can be used to obtain an expression of the coefficients d and z_0 of logarithmic law by applying equations (9) and (12) (Defina and Bixio, 2005).

$$\frac{d}{k} = 1 - \frac{1}{\kappa} \frac{\alpha_t u_k}{k u_*}, \quad (13)$$

$$\frac{z_0}{k} = \left(1 - \frac{d}{k} \right) \times \exp \left(-\kappa \frac{u_k}{u_*} \right). \quad (14)$$

2.4 Step 4 and 5: Implication for fish passage

For emergent blocks, the bulk velocity is directly deduced from equation (4) and the velocity between block is calculated with equation (1) to verify that it is lower than the fish swimming ability (criterion for fish passability). For submerged flows, the validity of l_0 , d/k and z_0/k is shown by the good agreement of the velocity profiles calculated and measured within and above the canopy (Fig. 4). The advantage of the proposed equations (Eqs. (10) and (11)) is that it establishes the conditions on the bed u_0 but also that it provides

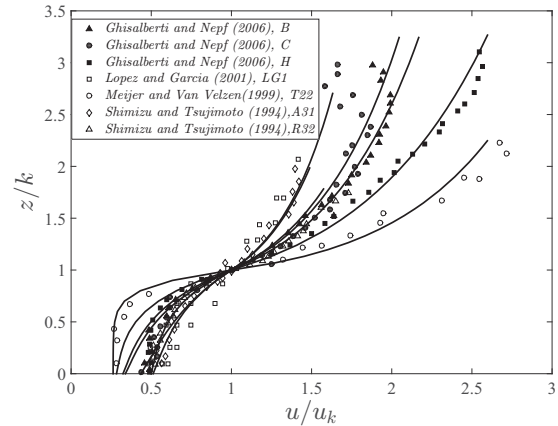


Fig. 4. Spatially double-averaged velocity profiles of experiments compared to the model, according to Ghisalberti and Nepf (2006) ($R^2 = 0.98, 0.92, 0.98$), Lopez and Garcia (2001) ($R^2 = 0.93$), Meijer and Velzen (1999) ($R^2 = 0.98$), Shimizu and Tsujimoto (1994) ($R^2 = 0.97, 0.95$). The model presented is in solid lines. The abbreviations correspond to experimental series.

an exponential profile near the canopy whose coefficients are determined by the way the obstacles are arranged. With equation (1), the maximal velocity within the block layer can be deduced from the vertical profile. Then, the location where the velocity is lower than swimming abilities is estimated.

The total discharge by unit width is obtained by the integration of the modeled velocity profiles. It must be sufficient to create an attracting current. Otherwise the same method has to be applied with lower concentration, steeper slope or considering submerged blocks.

3 Results and discussion

3.1 Emergent condition

In Figure 5, the assumption on $f_C(C)$ is confirmed by the comparison between this formula and those of Nepf (1999) and Idelcick (1986) for a set of vertical tubes. Then the stage-discharge relationship can be deduced from equation (4) where $f_C(C)$ is omitted but with a Froude number based on the bulk velocity V . This method avoids a complex function for $f_C(C)$ depending on a_y/a_x . The experimental results are analysed considering the bulk velocity both for the drag force and the bed friction. It is worth mentioning that knowing V_g remains important because it is the criterion for the fish passability and it fix the flow pattern by the Froude number.

Assuming $f_C = (V/V_g)^2$, the functions $f_F(F)$ and $f_{h_*}(h_*)$ are experimentally deduced. Their experimental values are obtained by considering the measured discharge and water-depth (F_0 and h_*) and equation (4).

We found that the correction function defined by Cassan et al. (2014) are still valid when $a_x \neq a_y$. When $h_* < 0.5$, the drag force and friction force have the same magnitude. As a consequence, the measurement error increases and the determination coefficients (R^2) are low (Fig. 6). This inaccuracy on C_d provides a weak variation of the total discharge because the bed friction is strong. In comparison with results obtained in Cassan et al. (2014) with a more accurate definition of f_C , the uncertainty of the model is slightly

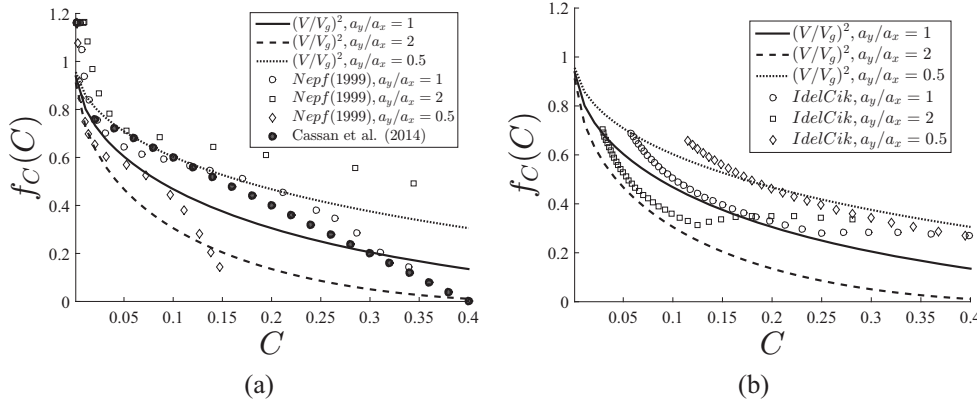


Fig. 5. Measured corrective function as a function of concentration compared with formula of Nepf (1999) (a) and Idelcick (1986) (b).

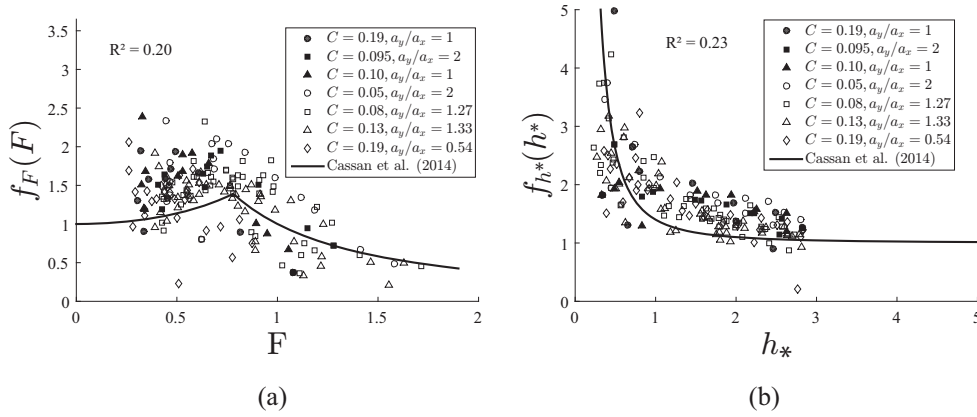


Fig. 6. Measured corrective function as a function of Froude number (a) and dimensionless water depth (b).

increased (around 10% in the range $0.1 < C < 0.25$) but the parameter C is now sufficient to characterize the geometry regardless of the ratio a_x/a_y . This remark is particularly important when the drag resistance is computed for an irregular arrangement of blocks or when the submerged flows model is applied.

Nevertheless, the maximal velocity is dependent on the ratio $f = a_x/a_y$. To quantify the influence of f , the model for emergent block is applied to a real scale fishway ($S = 0.05$, $D = 0.4$ m, $k_s = 0.1$ m, $C_{d0} = 1$). In Figure 7, it appears that reducing this ratio does not involve a significant increase of maximal velocity but it can lengthen the resting zone since a_y is higher than a_x . But, the velocity between two blocks becomes faster because the frontal area of blocks is larger at a given water depth. As it is shown that the stage-discharge relationship only changes with C the curves are plotted for a constant total discharge in the fish pass. A limitation to $f > 0.5$ can be proposed. Anyway for very low f value, the function f_C cannot be pertinent.

3.2 Submerged conditions

The experiments were used to determine the relationship between the geometric characteristic and l_0 . The l_0 value can be expressed experimentally using several approaches (Huthoff et al., 2007; Konings et al., 2012; Luhar et al., 2008; Nepf, 2012; Poggi et al., 2009). The present approach is a combination of these formulas in order to use a formula

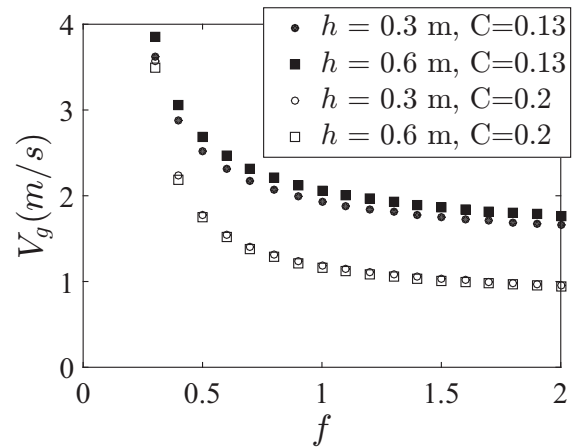


Fig. 7. Velocity between blocks as a function of the ratio a_x/a_y . Computation for a real scale fishway ($S = 0.05$, $D = 0.4$ m, $k_s = 0.1$ m, $C_{d0} = 1$).

available for a large range of macro-roughness arrangement. Unlike cases involving vegetation, k/D for macro-roughness is close to one. As a result, the influence of the bed is greater when the obstacles are shallow. Figure 8 shows the different possible configurations for each of the three length scales: s , k and D . To determine experimentally l_0 , the flow rate by integrating the calculated vertical velocity profile (steps 3c, 3d and 3e) is compared to the measured flow rate with an

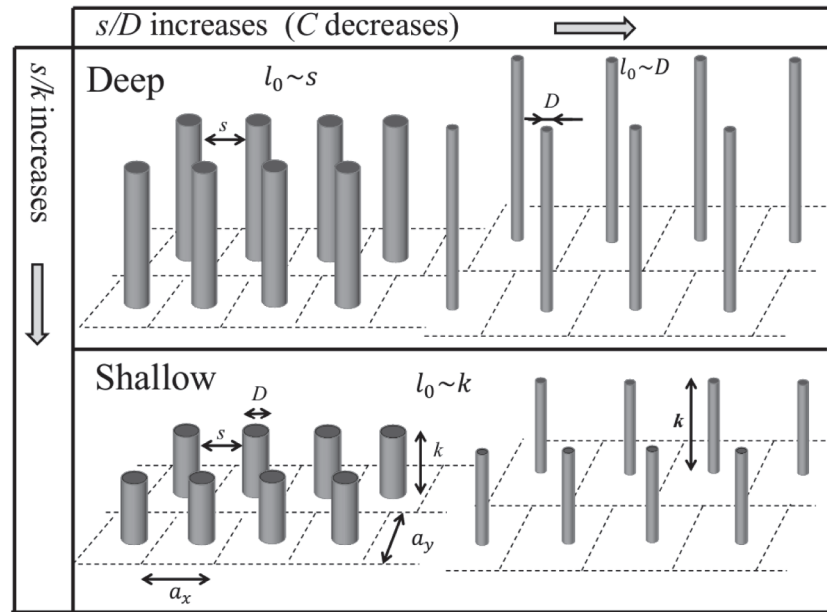
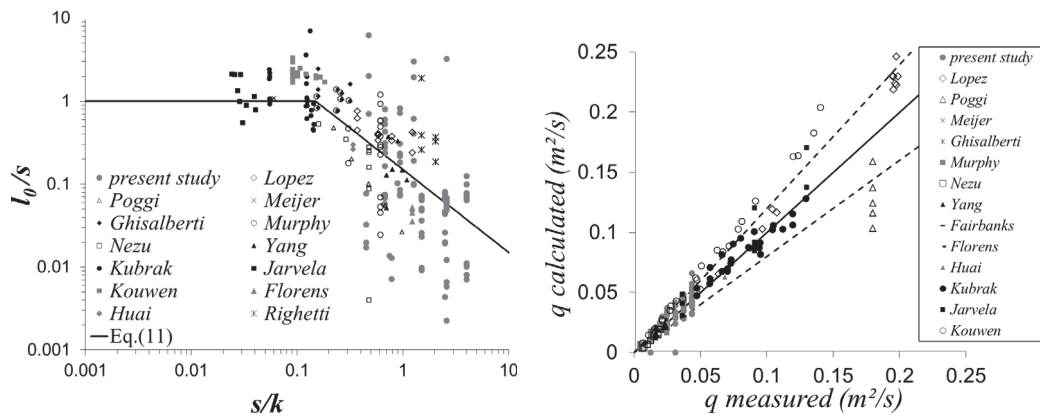


Fig. 8. Definition of lengths and turbulent length scale (l_0) as a function of blocks arrangement.



(a) Turbulent scale determined by comparing calculated and experimental discharge.

(b) Comparison of flow rates calculated with the model and measured flow rates per unit width. Dash lines represent error superior to 20%. $R^2=0.93$.

Fig. 9. Vegetation studies used to evaluate the model. Data from Lopez and Garcia (2001), Poggi *et al.* (2004), Meijer and Velzen (1999), Ghisalberti and Nepf (2006), Murphy and Nepf (2007), Nezu and Sanjou (2008), Yang and Choi (2009), Kubrak *et al.* (2008), Jarvela (2005), Kouwen and Unny (1969), Florens *et al.* (2013), Huai *et al.* (2009), Righetti and Armanini (2002).

optimization method (simplex algorithm from Matlab). For all experiments from literature (Kouwen and Unny, 1969; Meijer and Velzen, 1999; Lopez and Garcia, 2001; Righetti and Armanini, 2002; Poggi *et al.*, 2004; Jarvela, 2005; Ghisalberti and Nepf, 2006; Murphy and Nepf, 2007; Kubrak *et al.*, 2008; Nezu and Sanjou, 2008; Huai *et al.*, 2009; Yang and Choi, 2009; Florens *et al.*, 2013), C_d is considered equal to 1 if the block is circular and $C_d=2$ otherwise. The results performed by Poggi *et al.* (2009), Konings *et al.* (2012), Nezu and Sanjou (2008), Yang and Choi (2009), Huai *et al.* (2009), and Kubrak *et al.* (2008) are reused, together with those obtained specifically for the present study. As indicated by Konings *et al.* (2012), the experiments carried out with leafy vegetation behaved in a

particular way because of viscosity terms. The interpretation of l_0 is based on the assumptions of Belcher *et al.* (2003) and King *et al.* (2012). As expected, the experimental values of l_0 (Fig. 9) are similar to s when $s/k \ll 1$, and proportional to k when $s/k > 0.15$ which yields to equation (11).

Equation (11) is consistent with literature for shallow cases (Coccal and Belcher, 2004; Nikora *et al.*, 2013) or for deep cases (Ghisalberti and Nepf, 2006; Luhar *et al.*, 2008; Huai *et al.*, 2009; Poggi *et al.*, 2009). For all experiments considered, the averaged error between the experimental and computed (with equation (11)) discharge is about 20% as indicated by the dashlines in Figure 9b. For the experiments performed in this study, the averaged error is 15.8%.

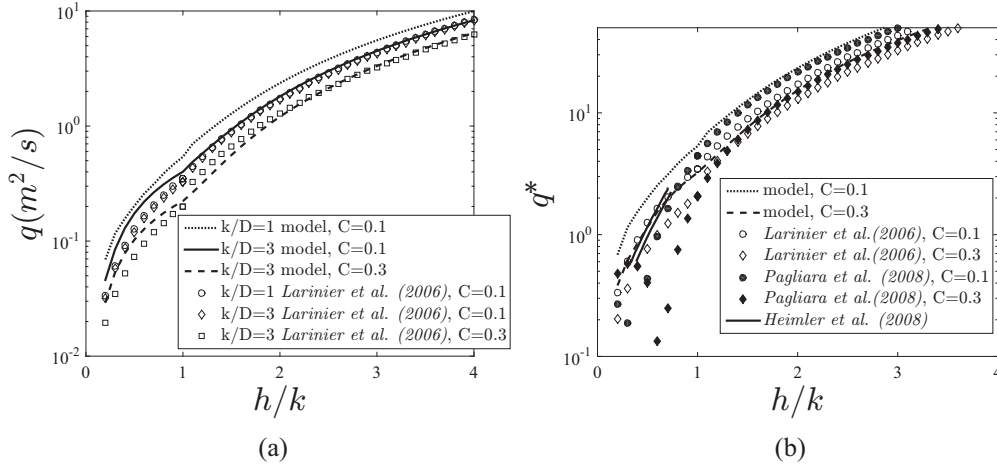


Fig. 10. Comparison of the stage-discharge relationship between the model and the empirical formula of [Larinier et al. \(2006b\)](#) (a) as a function of concentration and formula of [Larinier et al. \(2006b\)](#), [Heimerl et al. \(2008\)](#) and [Pagliara et al. \(2008\)](#) with $k/D = 1$ (b). Computation for a real scale fishway ($S = 0.05$, $D = 0.4$ m, $k_s = 0.1$ m, $C_{d0} = 1$).

3.3 Model validation

Lastly, the model is compared to the experimental correlation proposed by [Larinier et al. \(2006b\)](#) for rock-ramp fish passes (Eqs. (15) and (16)). This correlation is deduced from a statistical study of a large number of experiments in the laboratory, on cylindrical macro-roughness with $8\% < C < 16\%$, $1\% < S < 9\%$, $k = 0.07$ or 0.1 m and $D = 0.035$ m, the maximum ratio for h/k is 3.6.

For emergent conditions:

$$q = 0.815 \sqrt{gS} \left(\frac{h}{D} \right)^{1.45} C^{-0.456} D^{1.5}. \quad (15)$$

For submerged conditions:

$$q = 1.12 \sqrt{gS} \left(\frac{h}{D} \right)^{2.282} C^{-0.255} \left(\frac{k}{D} \right)^{-0.799} D^{1.5}. \quad (16)$$

The experimental correlation of [Pagliara et al. \(2008\)](#) is also used (for emergent and submerged conditions):

$$q = Vh = \sqrt{\frac{8ghS}{(-7.82S + 3.04)(1.4 \exp(-2.98C) + \ln(h/k))}} h. \quad (17)$$

The model results are consistent with the formula of [Larinier et al. \(2006b\)](#), including high concentrations (Fig. 10) superior to $C = 0.2$. However the model differs from statistical formulation for low value of k/D . Experimental data with $k/D < 1$ are used to calibrate the turbulence model whereas no such of experiments were used to establish the experimental correlation in [Larinier et al.'s \(2006\)](#) study. Similarly, equation (16) indicates that D has no influence except for C because only one diameter was used. In the presented model, D modifies the values of C_d , u_0 , s and then l_0 for deep cases. In Figure 10, the stage-discharge relationship is depicted for a real scale fishway. Comparison with other guidelines ([Larinier et al., 2006b](#); [Heimerl et al., 2008](#)) indicates that the model allows to reproducing experimental correlation between h_* and

$q_* = q/D^{5/2}$. The same dependence on C is found between the present study and results of [Pagliara et al. \(2008\)](#). For emergent performance, the model with high concentration $C = 0.3$ provides the same stage-discharge relationship than method from [Heimerl et al. \(2008\)](#). Therefore, the model is validated by other studies. But, as mentioned before, some advantages are added like the applicability to different shapes and the validity for a large range of geometry.

Moreover, the model allows estimating the double averaged velocity profile (Fig. 4) and turbulent shear stress (Eq. (7)) within and above the block layer whereas equations (16) and (17) only provide the total discharge. It is possible to know if hydrodynamic parameters are suitable with the swimming ability of fishes within the block layer even if the velocity is higher in the surface layer.

4 Conclusion

This paper presents an analytical model for calculating the stage-discharge relationship for emergent and submerged rock-ramp fish passes. New experiments are conducted to prove that results obtained by [Cassan et al. \(2014\)](#) are available whatever the block arrangement. For submerged blocks, canopy vegetation models are improved to take mixing length into account by linking it directly to the geometric characteristics of the arrangement. The model has been adjusted on the basis of a large number of experiments found in the literature as well as the presented fish passes configurations. The model seems to offer a good trade-off between its validity for a large range of geometrical arrangements and simplicity of use (number of parameters, calculation time, etc.). Although the mixing-length model provides few explanations about the structure of the turbulence, it can be used to estimate mean flow rate between and above the blocks fairly accurately. It is thus possible to predict the velocities that the different species of fish will need to overcome. It can also help to design effective and durable passes. The implementation of the model could be difficult but all equations can be solved with numerical tools. Software is developed currently and its ergonomics has been designed to help to use the presented flow chart.

Supplementary Material

The Supplementary Material is available at <http://www.kmae-journal.org/10.1051/kmae/2016032/olm>.

Acknowledgments. The research was supported by the ONEMA under the grant “Caractérisation des conditions hydrodynamiques dans les écoulements à fortes rugosités émergentes ou peu submergées”. This financial support is greatly appreciated.

NOTATIONS

α : ratio of the area where the bed friction occurs on $a_x \times a_y$
 α_t : turbulent length scale (m) within the blocks layer
 β : force ratio between drag and turbulent stress
 κ : von Karman's constant
 λ : frontal density
 σ : ratio between the block area in the x, y plane and D^2
 ξ : dimensionless square of the velocity
 a_x : width of a cell (perpendicular to flow) (m)
 a_y : length of a cell (parallel to flow) (m)
 C : blocks concentration
 C_{d0} : drag coefficient of a block considering a single block infinitely high with $F \ll 1$
 C_d : drag coefficient of a block under the actual flow conditions
 C_f : bed-friction coefficient
 d : zero-plane displacement of the logarithmic profile (m)
 D : characteristic width facing the flow (m)
 F : Froude number based on h and V_g
 F_0 : Froude number based on h and V
 g : gravitational constant (m s^{-2})
 h : mean water depth in a cell (m)
 h^* : dimensionless water depth (h/D)
 k : height of blocks (m)
 k_s : height of roughness (m)
 l_0 : turbulent length scale (m) at the top of blocks (m)
 N : ratio between bed friction force and drag force
 q : specific discharge per unit width ($\text{m}^2 \text{s}^{-1}$)
 q^* : specific discharge per unit width ($\text{m}^{-0.5} \text{s}^{-1}$)
 Re : Reynolds number based on k and u_0
 R^2 : determination coefficient
 s : minimum distance between blocks
 S : bed slope
 u : averaged velocity at a given vertical position (m s^{-1})
 u_0 : averaged velocity at the bed (m s^{-1})
 u_k : averaged velocity at the top of blocks (m s^{-1})
 u^* : shear velocity (m s^{-1})
 V_g : averaged velocity in the section between two blocks (m s^{-1})
 V : bulk velocity (m s^{-1})
 z : vertical position (m)
 z_0 : hydraulic roughness (m)
 \tilde{z} : dimensionless vertical position

References

- Baki A, Zhu D, Rajaratnam N. 2014. Mean flow characteristics in a rock-ramp-type fish pass. *J Hydraul Eng* 140 (2): 156–168.
- Belcher SE, Jerram N, Hunt JCR. 2003. Adjustment of a turbulent boundary layer to a canopy of roughness elements. *J Fluid Mech* 488: 369–398.
- Cassan L, Tien T, Courret D, Laurens P, Dartus D. 2014. Hydraulic resistance of emergent macroroughness at large Froude numbers: design of nature-like fishpasses. *J Hydraul Eng* 140 (9): 04014043.
- Coccal O, Belcher SE. 2004. A canopy model of mean winds through urban areas. *Q J R Meteorol Soc* 130 (599): 1349–1372.
- Defina A, Bixio A. 2005. Mean flow turbulence in vegetated open channel flow. *Water Resour Res* 41: 1–12.
- FAO. 2002. Fish passes – design, dimensions and monitoring. Rome: FAO, 138 p.
- Florens E, Eiff O, Moulin F. 2013. Defining the roughness sublayer and its turbulence statistics. *Exp Fluids* 54 (4): 1–15.
- Ghisalberti M, Nepf HM. 2006. The structure of the shear layer in flows over rigid and flexible canopies. *Environ Fluid Mech* 6: 277–301.
- Heimerl S, Krueger F, Wurster H. 2008. Dimensioning of fish passage structures with perturbation boulders. *Hydrobiologia* 609 (1): 197–204.
- Huai W-x, Chen Z-b, Han J, Zhang L-x, Zeng Y-h. 2009. Mathematical model for the flow with submerged and emerged rigid vegetation. *J Hydrodyn B* 21 (5): 722–729.
- Huthoff F, Augustijn DCM, Hulscher SJMH. 2007. Analytical solution of the depth-averaged flow velocity in case of submerged rigid cylindrical vegetation. *Water Resour Res* 43 (6): W06413
- Idelcick IE. 1986. Mémento des pertes de charges. 3e édition. Eyrolles, EDF.
- Jarvela J. 2005. Effect of submerged flexible vegetation on flow structure and resistance. *J Hydrol* 307 (1–4): 233–241.
- Katul GG, Poggi D, Ridolfi L. 2011. A flow resistance model for assessing the impact of vegetation on flood routing mechanics. *Water Resour Res* 47 (8): 1–15.
- King AT, Tinoco RO, Cowen EA. 2012. A k - ϵ turbulence model based on the scales of vertical shear and stem wakes valid for emergent and submerged vegetated flows. *J Fluid Mech* 701: 1–39.
- Klopstra D, Barneveld H, van Noortwijk J, van Velzen E. 1997. Analytical model for hydraulic resistance of submerged vegetation. In: *Proceedings of the 27th IAHR Congress*, pp. 775–780.
- Konings AG, Katul GG, Thompson SE. 2012. A phenomenological model for the flow resistance over submerged vegetation. *Water Resour Res* 48 (2).
- Kouwen N, Unny TE. 1969. Flow retardance in vegetated channels. *J Irrigat Drain Div* 95 (2): 329–344.
- Kubrak E, Kubrak J, Rowinski PM. 2008. Vertical velocity distributions through and above submerged, flexible vegetation. *Hydrol Sci J* 53 (4): 905–920.
- Larinier M, Travade F, Porcher JP. 2006. Fishways: biological basis, design criteria and monitoring. *Bull Fr Peche Piscic* 364 (Suppl.): 208 p. ISBN 92-5-104665-4.
- Larinier M, Courret D, Gomes P. 2006. Technical Guide to the Concept on nature-like Fishways. Rapport GHAAPE RA.06.05-V1, 5 (in French).
- Lopez F, Garcia M. 2001. Mean flow and turbulence structure of open-channel flow through non-emergent vegetation. *J Hydraul Eng* 127 (5): 392–402.

- Luhar M, Rominger J, Nepf H. 2008. Interaction between flow, transport and vegetation spatial structure. *Environ Fluid Mech* 8: 423–439.
- Meijer DG, Velzen EHV. 1999. Prototype scale flume experiments on hydraulic roughness of submerged vegetation. In: *28th International Conference, Int. Assoc. of Hydraul. Eng. and Res., Graz, Austria*.
- Murphy EG, Nepf H. 2007. Model and laboratory study of dispersion in flows with submerged vegetation. *Water Resour Res* 43 (5): 1–12.
- Nepf HM. 1999. Drag, turbulence, and diffusion in flow through emergent vegetation. *Water Resour Res* 35 (2): 479–489.
- Nepf HM. 2012. Hydrodynamics of vegetated channels. *J Hydraul Res* 50 (3): 262–279.
- Nezu I, Sanjou M. 2008. Turbulence structure and coherent motion in vegetated canopy open-channel flows. *J Hydro-Environ Res* 2 (2): 62–90.
- Nikora N, Nikora V, O'Donoghue T. 2013. Velocity profiles in vegetated open-channel flows: combined effects of multiple mechanisms. *J Hydraul Eng* 139 (10): 1021–1032.
- Nikora V, Goring D, McEwan I, Griffiths G. 2001. Spatially averaged open-channel flow over rough bed. *J Hydraul Eng* 127 (2): 123–133.
- Pagliara S, Das R, Carnacina I. 2008. Flow resistance in large-scale roughness conditions. *Can J Civil Eng* 35: 1285–1293.
- Poggi D, Krug C, Katul GG. 2009. Hydraulic resistance of submerged rigid vegetation derived from first-order closure models. *Water Resour Res* 45 (10).
- Poggi D, Porporato A, Ridolfi L. 2004. The effect of vegetation density on canopy sub-layer turbulence. *Bound-Layer Meteorol* 111: 565–587.
- Rice C, Kadavy K, Robinson K. 1998. Roughness of loose rock riprap on steep slopes. *J Hydraul Eng* 124 (2): 179–185.
- Righetti M, Armanini A. 2002. Flow resistance in open channel flows with sparsely distributed bushes. *J Hydrol* 269 (1–2): 55–64.
- Shimizu Y, Tsujimoto T. 1994. Numerical analysis of turbulent open-channel flow over vegetation layer using a k-ε turbulence model. *J Hydrosc Hydraul Eng* 11 (2): 57–67.
- Tran DT. 2015. Metrologie et modelisation des écoulements a forte pente autour d'obstacles: application au dimensionnement des passes naturelles, Ph.D. thesis, INPT (in French).
- Yang W, Choi S-U. 2009. Impact of stem flexibility on mean flow and turbulence structure in depth-limited open channel flows with submerged vegetation. *J Hydraul Res* 47 (4): 445–454.

Cite this article as: Cassan L, Laurens P. 2016. Design of emergent and submerged rock-ramp fish passes. *Knowl. Manag. Aquat. Ecosyst.*, 417, 45.